



# Experimental Investigation of Turbidity Flow in 90 Degree Bend with Mobile Bed

Marzieh Mohammadi<sup>1,\*</sup>, Mehdi Ghomeshi<sup>2</sup>

<sup>1</sup>PHD student of hydraulic structure, Faculty of Water Sciences Engineering, Shahid Chamran Ahvaz University, Ahvaz, Iran

<sup>2</sup>Professor of hydraulic structure, Faculty of Water Sciences Engineering, Shahid Chamran Ahvaz University, Ahvaz, Iran

\*Corresponding Author E-mail: [Mohamadi\\_200035@yahoo.com](mailto:Mohamadi_200035@yahoo.com)

Received: 10 April 2019, Revised: 19 May 2019, Accepted: 19 June 2019

## ABSTRACT

Turbidity currents in the ocean and lakes are driven by suspended sediment. The vertical profiles of velocity and excess density are shaped by the interaction between the current and the bed as well as between the current and the ambient water. This paper presents 48 series of experiments in which saline gravity currents flow through a laboratory sinuous flume. This flume contains three successive bends with three different relative curvature radiuses:  $R/B=2, 4$  and  $6$ ,  $8.5$  m length,  $20$  cm width and  $70$  cm height. Experiments were performed by four discharges ( $0.7, 1, 1.5, 2$  lit/s) and four concentrations ( $10, 15, 20, 25$  gr/lit). An Acoustic Doppler Velocity meter (ADV) was used to record the local velocity. According to the results of experiments on the mobile bed, increasing the concentration of the incoming flow, the flow velocity of the fluid, is also increased and, the maximum velocity occurs near the bed instead of the top of the current. The important point in the flow rate profiles is that the rate of increase in velocity depends on changes in the form of the bed due to the increase in concentration. By increasing the concentrations of turbidity flow, the shear stress of the bed is also increased. Therefore, the rate of increase in velocity will occur by removing the bed forms and reducing the roughness and shear stress of the bed. Thus, increasing the concentration increases the power of the current. Thus, at the beginning, the roughness and shear stress of the bed increased and, then, by removal of bed forms shear stress decreased.

**Key words:** Turbidity currents, Mobile bed, Flow profiles, Bend.

## Introduction

Turbidity currents are a variety of subaqueous sediment-gravity flows, in which the suspension of sediment by water turbulence produces a water-sediment mixture that is denser than the ambient water and hence flows due to gravity along a topographic gradient. This type of sediment gravity flow is the most important mechanism for the movement and deposition of sand on deep-sea floors, as well as on the underwater slopes of many deltas and lakes (Figure 1). The hydrodynamics of turbidity currents are difficult to study in the natural environments,

whereas laboratory experiments are limited to small-scale flows, time-consuming and not necessarily easier when it comes to the measuring of flow properties and establishing the relationships between the turbulent flow structure and the transport and deposition of sediment.

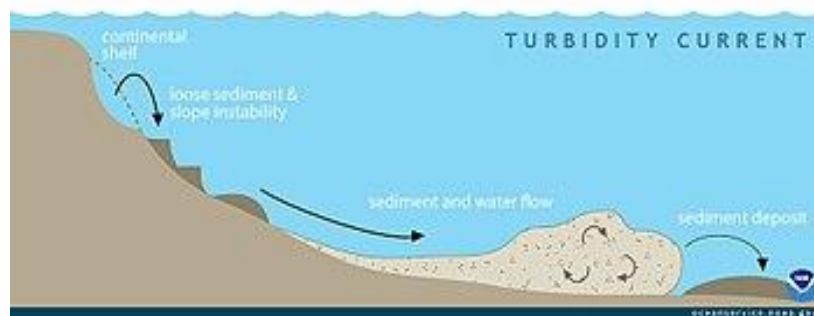


**Figure 1.** Longitudinal section through an underwater turbidity flow (Smith and Möller, 2003)

The term turbidity current was introduced by Johnson (1938) to define a current due to turbid or muddy water. Etymologically, 'turbidity current' means water flow driven by sediment, or simply turbid flow (*i.e.*, a water flow rendered opaque by suspended sediment) (Smith and Möller, 2003). A widely accepted definition in reference (Middleton, 1966) says that 'turbidity currents are sediment-gravity flows in which the sediment is supported mainly by the upward component of fluid turbulence. In reference (Altinakar *et al.*, 1996), it simultaneously considers the density difference between the flow and the ambient water, and hence regards the sediment-gravity flows as the 'high-density' end-member in the spectrum of density flows. On the basis of this latter criterion of flow/ambient density difference, the density flows are categorized as (Figure 2). 1) hypopycnal flows; 2) homopycnal flows; 3) mesopycnal flows; and 4) hyperpycnal flows.

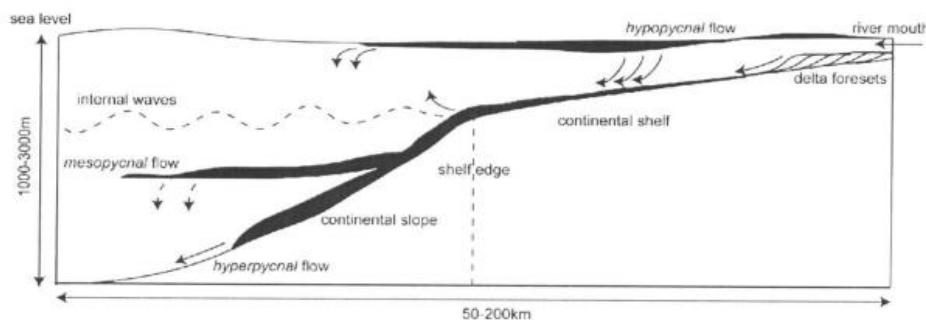


**Figure 2.** Four types of density flow and their occurrence in a continental-margin setting (Smith and Möller, 2003). Arrows are used to indicate direction of transport, settling and suspension of sediment

In accordance to the original terminology, flows with a density lower than that of ambient water are called 'hypopycnal' flows (overflows). Hypopycnal flows occur primarily at river mouths, where sediment is dispersed as a buoyant plume (Buckee *et al.*, 2001). The negative difference in density between the river effluent and the ambient water is usually caused by the differences in temperature and salinity between the river water and the seawater of the basin, which are more significant than the positive difference in density caused by sediment suspension. Turbidity currents are described to have a well-defined head, body and tail, and in some cases also a

thinner neck linking the head with the body (Middleton, 1966). The dynamics of the head are particularly important, because they set the boundary condition for the current as a whole (Altinakar *et al.*, 1996; Buckee *et al.*, 2001; Winn and Dott, 1977) as they have pointed out that the head is a locus for erosion, and hence of primary sediment logical importance. The head has an overhanging snout as a result of the no-slip condition at the lower boundary and frictional resistance at the upper boundary (Figure 3). The no-slip condition requires that the velocity must decrease to zero at the boundary between the fluid and the stationary substrate. At the rear of the head, a series of transverse vortices (billows) was developed and identified as a product of the Kelvin-Helmholtz instabilities (Smith and Möller, 2003).

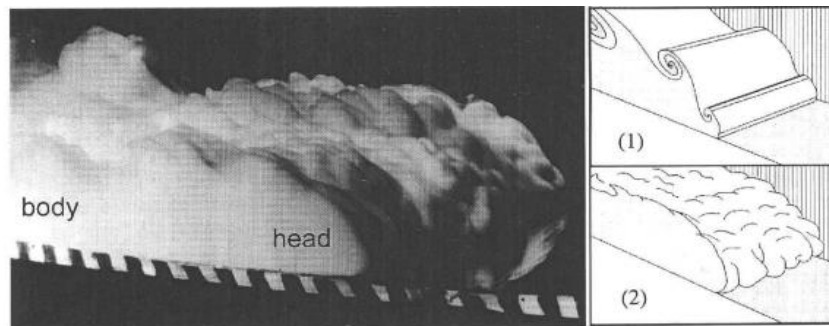


**Figure 3.** Laboratory flume photograph showing the frontal part of an experimental turbidity current, with sketches showing the Kelvin-Helmholtz billows (1) and frontal lobes and clefts (2). (Smith and Möller, 2003)

(Winn and Dott, 1977) Describes gravel bed forms emplaced by the bed-load component of turbidity currents flowing in a confined channel in the Cerro Toro formation of southern Chile. At field scale, (Xu *et al.*, 2004) measured vertical velocity profiles within the Monterey Submarine Canyon. In the laboratory, previous experimental studies have documented the vertical structure of the body of gravity flows. Among them are those by (Ellison and Turner, 1959; Lofquist, 1960; Middleton, 1966; García, 1993; García, 1994; Altinakar *et al.*, 1996; Kneller *et al.*, 1999, Buckee *et al.*, 2001). Only some of these studies were performed over mobile beds, and, then, when bed forms developed, their influence on the flow was not evaluated. Bed forms have feedback mechanisms, and in turn, affect the flows that originally created them [García and Parker, 1993]. Observed bed forms were created by turbidity and saline currents moving over sediment beds, but no specific attention was devoted to their effects on the currents. Understanding the variability of the internal structure of turbidity currents across the range of Froude Numbers and regimes of bed forms is important as it is related to the depositional sequences of sediment as observed in the experiments, [García, 1993; García, 1994; Sequeiros *et al.*, 2009) that eventually determine the potential for hydrocarbon reservoirs in submarine fans.

## Materials and methods

### Theoretical or Experimental Modeling

#### Experimental Set Up

The types of gravity flows were studied: flows which obtained their driving force from dissolved salt (48 experiments). One grade of particles was used for bed material with the value of  $d_{50}$ , 450 micro meter, and specifications of bed sediment were presented in Table 1. It was Polystyrene

with a specific gravity of 1.07 (Figure 4). The experiments were carried out in a flume with three different relative curvature radiuses:  $r/b=2, 4$  and  $6$  and  $8.5$  m long,  $20$  cm wide and  $0.7$  m deep, with  $0.001$  bottom slope at the Shahid Chamran University of Ahvaz, in Hydraulic Laboratory (Figure 5). The tank was initially filled with fresh water. Dense mixtures of water and salt were fed into the flume from a  $2$  m<sup>3</sup> mixing tank by means of a pump (Figure 6). The discharge rate was measured by a magnetic McCrometer Flowmeter with a capacity up to  $20$  l/sec<sup>1</sup>. A diffuser ensured that the mixture of saline water was injected uniformly along the flume width at its upstream end. The diffuser was located just upstream of a gate which guided the mixture to the bottom of the flume. A layer of bed sediment was placed on the bed and leveled to a constant thickness before each run. Elevation or thickness of turbidity flow was measured by rulers that stick in each bend (Figure 7). This sediment served as the source for bed load. In the case of runs 1 to 48, the bed slope was stable. All of these flows turned out to be supercritical in the sense of the densimetric Froude Number. An inset damping tank is located at the downstream end of the flume. The bottom current fell over the invert of the damping tank, and was then pumped out to prevent current back up. A supply of fresh water from the top of the damping tank in conjunction with an overflow device guaranteed the maintenance of a constant level of fresh water in the flume.

**Table 1.** Specifications of bed sediment tested

Sediment type	EPS
Sediment density* (kg/m <sup>3</sup> )	1070
sediment average diameter (d <sub>50</sub> μm)	450
Sediment diameter (d <sub>90</sub> μm)	660
Geometric standard deviation (σ <sub>g</sub> )	1.4



**Figure 4.** Mobile bed Polystyrene material

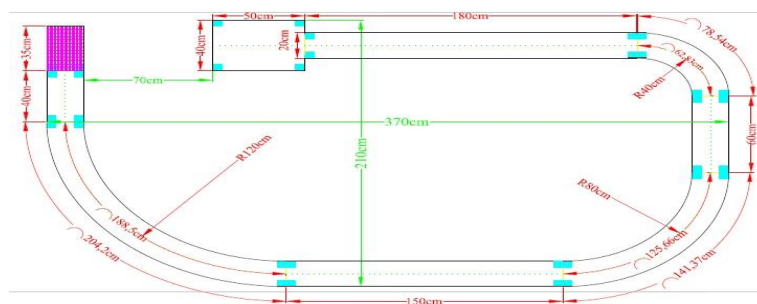


**Figure 5.** Sketch of experimental flume. Length units are in centimeters

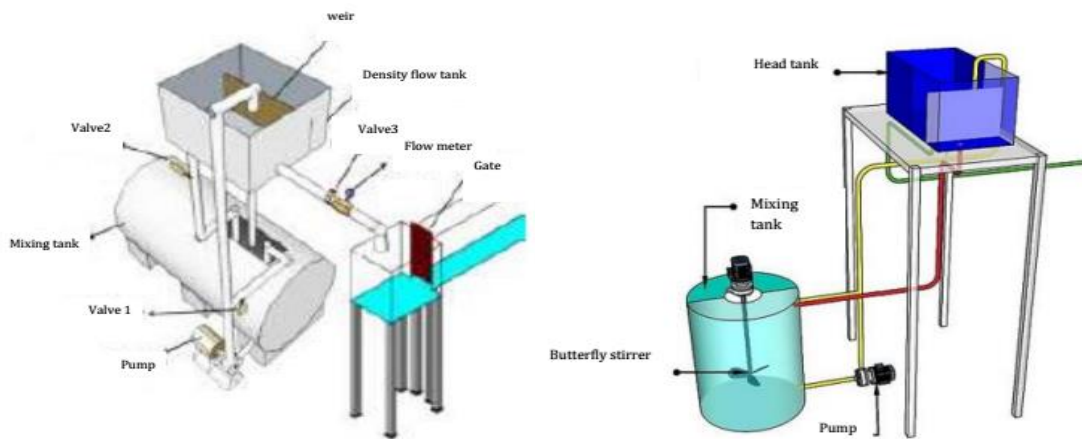


**Figure 6.** Mixing tank by means of a pump



**Figure 7.** Elevation Measurement

A set of siphons located at the 10 cm after beginning of each bend and 10 point before the ending of the each bend was used to obtain flow samples at different elevations in order to derive profiles of salinity (Figure 8). Each set sustain 14 tubes and was positioned so that the siphons were 1 cm above the bed at the beginning of each test. The types of siphons were made of aluminum with 4 mm external diameter and 3 mm internal diameter. The collected samples were transported to laboratory quality to measure salt concentration.

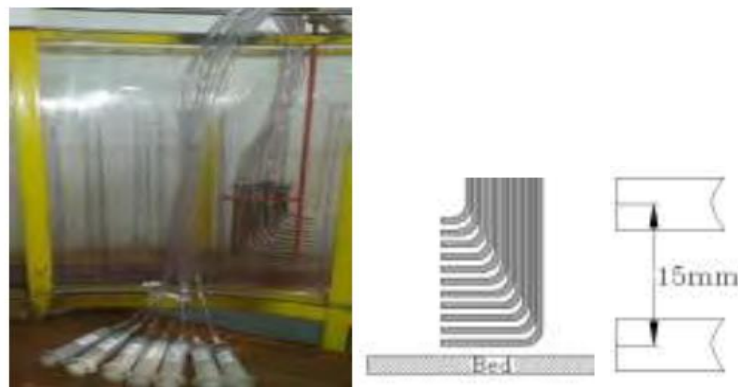


**Figure 8.** Rakes of siphons located in flume

Velocity profiles were taken with three-dimensional velocity measurements (Acoustic Doppler Velocity meter) (ADV). The probe has three arms corresponding to the  $x$ ,  $y$ , and  $z$  axis which relate to the downstream, lateral, and vertical flow directions, respectively, due to cart orientation. Acoustic Doppler Velocity meter works by emitting an acoustic burst into the water column, where the signal is reflected off of the suspended particles to the three corresponding arms as depicted in (Figure 9).

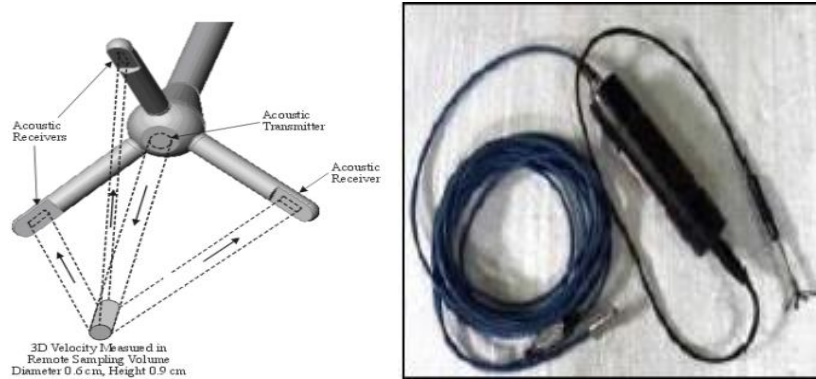


**Figure 9.** ADV measurement principles

Travel times of the acoustic signal are post-processed to determine velocities. Velocity measurements were recorded by a personal computer and the Horizon ADV program at a rate of 25 Hz over a period of 60 seconds. The ADV probe was mounted on a standard point gage to ensure accuracy of the testing locations in the water column. The sampling volume was located 0.164 ft (5 cm) below the acoustic transmitter, which hindered measurements in the upper portion of the water column at low flow depths. An example flow depth less than 1.64 ft would limit data collection at the 10% depth location. Maximum stream wise velocities ranged from 11 to 40 cm sec). The ADV was connected to a Velmex vertical positioning electric slide (Velmex Inc., Bloomfield, NY, USA) allowing accurate vertical displacements (<0.03 mm). The ADV and its electric arm were mounted on a rolling horizontal platform that could be translated to capture velocity profiles at various locations while the ADV measured velocities of saline currents suitably.

### Characteristics of the flows

Turbidity currents can be erosive or depositional. The flow itself is taken to be essentially two dimensional. Some examples for turbidity currents besides hydraulics are dust storms in deserts, pyroclastic flows of volcanos, powder-snow avalanches and large scale marine turbidity currents resulting from land slides. Density currents will reach a normal state within a short distance. In a normal state, gravity force, bottom shear, pressure force and momentum due to water entrainment are in balance.

The Richardson Number assumes a normal value after a short distance. In turbidity currents, there are additional terms in the governing equations (erosion, deposition). The Richardson Number was given as:

$$Ri = \frac{g' h_p}{u_p^2}, \quad g' = \frac{\Delta \rho}{\rho_a} g \quad (1)$$

where  $g = 980 \text{ cm/s}^2$ ,  $\Delta\rho = \rho_s - \rho_a$ , density difference between ambient and dense fluid, and  $\rho_s$  is the density of the gravity flow,  $\rho_a$  is the ambient fluid density, the peak velocity  $u_p$  and the distance above the bed  $h_p$  where this velocity is realized.

The measurements described above allowed the determination of locally averaged stream wise flow velocity  $u$  and fractional excess density  $fe$  as functions of the upward normal coordinate  $z$ . Here, fractional excess density  $fe$  is given as:

$$fe = \frac{\Delta\rho}{\rho_a} \tag{2}$$

where  $\rho_a$  is the density of the ambient (salt-free, sediment-free) water and  $\Delta\rho$  is the difference in density between the flow and the ambient water. Six parameters that are used below were calculated from profiles such as those of (Figure 10).

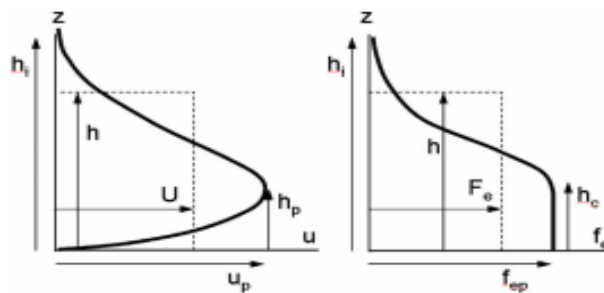


**Figure 10.** Main parameters used to classify gravity flows from velocity and excess density profiles

the peak velocity  $u_p$  and the distance above the bed  $h_p$  where this velocity is realized, a flow layer thickness  $h$ , layer-averaged flow velocity  $U$  and a layer-averaged fractional excess density  $Fe$  and, finally, a bed shear velocity  $u^*$ . The method for the determination of  $u^*$  is presented in the following section. The parameters  $h$ ,  $U$  and  $Fe$  were determined from the moment equations introduced by (Ellison and Turner, 1959):

$$\bar{U}h = \int_0^\infty u dz \tag{3}$$

$$\bar{U}^2 h = \int_0^\infty u^2 dz \tag{4}$$

$$\bar{U}F_e h = \int_0^\infty u f_e dz \tag{5}$$

In the above three equations, the upper limit  $\infty$  was replaced by the distance from the bed to the interface between the current and the ambient water where, in all cases,  $u$  and  $Fe$  were very small so the Densimetric Froude Number is given as:

$$Fr_d = \frac{u}{\sqrt{g'h}} \tag{6}$$

**Determination of bed shear stress in direct way**

In the case of equilibrium open-channel flows, the bed shear stress  $\tau_b$  and the bed shear velocity  $u^*$  can be determined from the relation:

$$\tau_b = \rho u_*^2 = \rho g h s \quad (7)$$

Where in the above Eq.  $h$  denotes flow depth. The above relation cannot, however, be used for density underflows, due to (among other factors) entrainment of ambient water across the interface. With this in mind, shear velocity  $u$  was computed from the velocity profiles below the peak velocity:

$$u_* = k \frac{n \sum u_i \ln z_i - \sum u_i \sum \ln z_i}{n \sum \ln^2 z_i - (\sum \ln z_i)^2} \quad (8)$$

Here,  $n$  is the number of measuring points used in the regression.

### Determination of bed shear stress in bend

Bends in meandering streams have been examined by researchers for decades to understand the distribution of velocity and shear stress and its effect on bend migration (Chen and Shen, 1984). Complex nature of flow in bends is influenced by channel geometry characteristics, flow characteristics, and fluid and sediment properties (Parker *et al.*, 1986). Shear stresses are directly affected by local accelerating, decelerating, and secondary flows (Ippen *et al.*, 1960). By isolating variables, researchers have developed relationships between boundary shear stress and geometric characteristics. Shear stress estimates by Reynolds stresses have been determined in cases where one-dimensional flows were not assumed thereby incorporating a stress component acting in the transverse direction. (Huthnance *et al.*, 2002) determined bed shear stress in an oceanographic study utilizing velocity fluctuations acting on the vertical plane in the downstream and transverse directions as seen in Eq. (9). It was noted that the method is highly sensitive to measurement of vertical velocity fluctuations but was more reliable than the logarithmic distribution. (Tilston, 2005) Used the method in a meandering bend but cautioned results may be misleading as the resulting magnitude accommodates stresses acting in a direction opposite that of the primary:

$$\tau = \rho (\overline{w'u'^2} + \overline{w'v'^2}) \quad (9)$$

where:  $\tau$ =shear stress;  $\rho$ =mass density;  $u'w'$ =covariance of velocity fluctuations in the stream-wise and vertical flow directions; and  $v'w'$ =covariance of velocity fluctuations in the transverse and vertical flow directions.

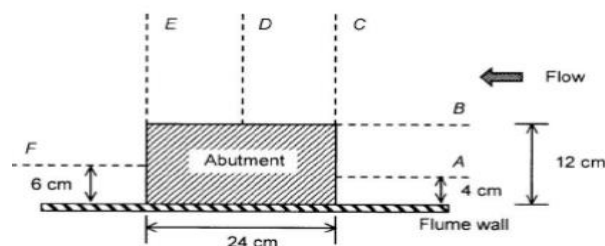


**Figure 11.** Measurement sections around abutment (Dey and Barbhuiya, 2005)

(Dey and Barbhuiya, 2005) used a combination of Reynolds stresses in determining bed shear near a vertical-wall abutment for pre- and post-scour conditions. Bed shear stress

was determined by Eq. (10) or Eq. (11), depending on the location near the abutment as presented in Figure 11. Eq. (10) was used to determine boundary shear stress for Sections A, B, and F and Eq. (11) for Sections C, D, and E (Dey and Barbhuiya, 2005):

$$\tau_o = \sqrt{\tau_y^2 + (\tau_x \cos\phi b + \tau_z \sin\phi b)^2} \quad (10)$$

$$\tau_o = \sqrt{\tau_x^2 + (\tau_y \cos\phi b + \tau_z \sin\phi b)^2} \quad (11)$$

where:  $\tau_o$ =bed shear stress;  $\tau_y = -\rho(u'v' + w'v')$ , where  $\rho$ =mass density of water;  $\tau_x = -\rho(w'u' + v'u')$ ;  $\tau_z = -\rho(u'w' + v'w')$ ; and  $\phi b$ =local angle of the scoured bed with the horizontal (equals 0 for plane bed).

Although it is not explicitly stated, it appears that (Dey and Barbhuiya, 2005) used a single near-bed measurement for bed shear stress determination. (Duan, 2009) used the same principle as that of (Dey and Barbhuiya, 2005) in a similar straight-flume flat-bed experimental study with a dike in the flow field. Assuming a flat bed reduces Eq. (11) to below Equation:

$$\tau_o = \sqrt{(\tau_b^x)^2 + (\tau_b^y)^2} \quad (12)$$

Where:  $\tau_o$ =bed shear stress;  $\tau_b^x = -\rho(w'u' + v'u')$ ,  $\rho$ =mass density of water; and  $\tau_b^y = -\rho(w'v' + u'v')$ .

### Stream Morphology in Bends

Drawings of a straight and a meandering channel are presented in (Figure 12) Pool-riffle sequences are the characteristics of cobble, gravel, and mixed-load rivers of moderate gradient (smaller than 5%) (Sear, 1996). Topographic high points are defined as riffles and low points are defined as pools (Watson *et al.*, 2005). The grain sizes found in riffles are larger than those found in pools. In reference (Keller, 1971), it was explained that the reason for the difference in grain size is caused by the sorting process. In addition, it explained that fine sediments are removed from riffles during low flows due to flow velocity and shear stress. These sediments are then deposited in pools. Normally, the outside bank is deeper than the inside bank, forming a point bar at the inside bank.

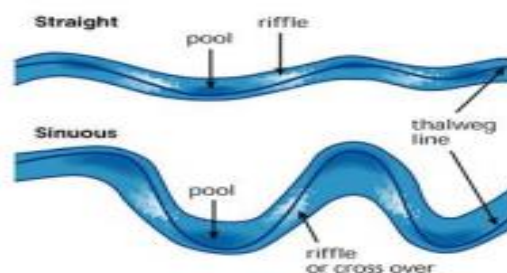


**Figure 12.** Graphic Description of a Straight Channel and a Meandering Channel (Richardson and etal, 2001)

## Transverse Velocity Distribution in Bends

Imbalance in radial pressure around the bend causes the transverse velocity distribution in a meandering channel (Richardson and etal, 2001). (Figure 13) represents a typical cross section within a bend and the vertical distribution of longitudinal velocity. The radial forces that act on the shaded control volume (Figure 13 (a)) are the centrifugal force that was presented in Eq. 13:

$$F_c = \frac{mv^2}{r} \quad (13)$$

Where:  $F_c$  = centrifugal force [N.m/s<sup>2</sup>];  $m$  = mass of the moving object [N];  $v$  = moving velocity of the object [m/s]; and  $r$  = value of the radius of curvature [m].

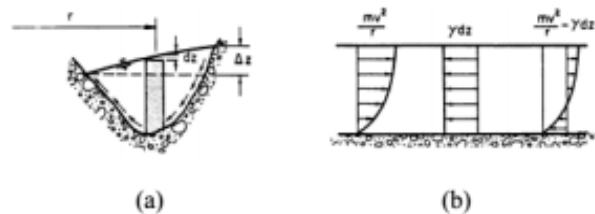


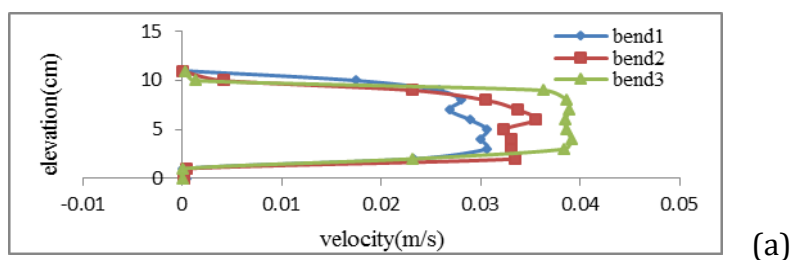
**Figure 13.** Schematic Descriptions of Flow in a Meandering Channel (Richardson and etal, 2001)

In addition, super elevation of the water surface ( $dz$ ) results in the differential hydrostatic force ( $\gamma dz$ ). Therefore, the centrifugal force is very near the surface where the flow velocity is greater and less at the bed where the flow velocity is small (Richardson and etal, 2001). The differential hydrostatic force is constant throughout the depth of the control volume. (Figure 13 (b)) explains that the combination of centrifugal force and hydrostatic force causes a secondary flow in the bend (Richardson and etal, 2001).

## Results and discussion

The primary goal of this experiment was to characterize the patterns of turbidity currents moving through a sinuous channel with mobile bed. We were particularly determining how channel curvature, distance from the source, and the relative thickness of currents changed the patterns of turbidity current, both inside and outside of the channel over mobile bed.

Bed resistance relations based on: (i) the peak flow velocity; (ii) the height above the bed at which this peak is attained; and (iii) the bed roughness height. The upper layer of flow is shaped predominantly by shear stresses exerted in the vicinity of the interface, with the consequent entrainment of ambient fluid and mixing fluid. The lower layer is also affected by shear stress exerted at the bed which mixes the flow, thus raising the position of the velocity peak and making density profiles more homogeneous below the peak (Figure 15).



(a)

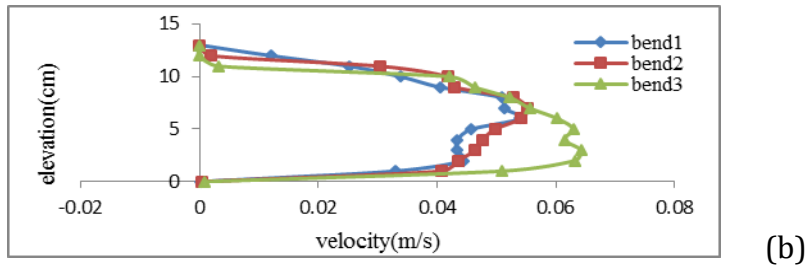


**Figure 15.** Longitudinal Velocity Profile in bend with R/B=2, R/B=4 and R/B=6: (a) Q=0.7l/s and C=15 gr/l (b) Q=2 l/s and C=15 gr/l

The experiments showed that, by moving the flow along the bend, the depth of flow along the inner wall decreases and increases along the outer wall. In the vicinity of the inner wall, a negative longitudinal pressure gradient occurs and accelerates the particles. In the opposite direction, near the outer wall of the gradient, the pressure is longitudinally positive and the pressure along the flow is increased. Based on the results obtained in the first bend with R/B=2 and the second cross section (middle bend), the maximum velocity is toward the inner wall (Figure 16). This is true of other concentrations. As the flow enters the bend due to the sudden change in the curvature and the effect of the centrifugal force along the inner wall, the pressure is decreased and along the outer wall increases.

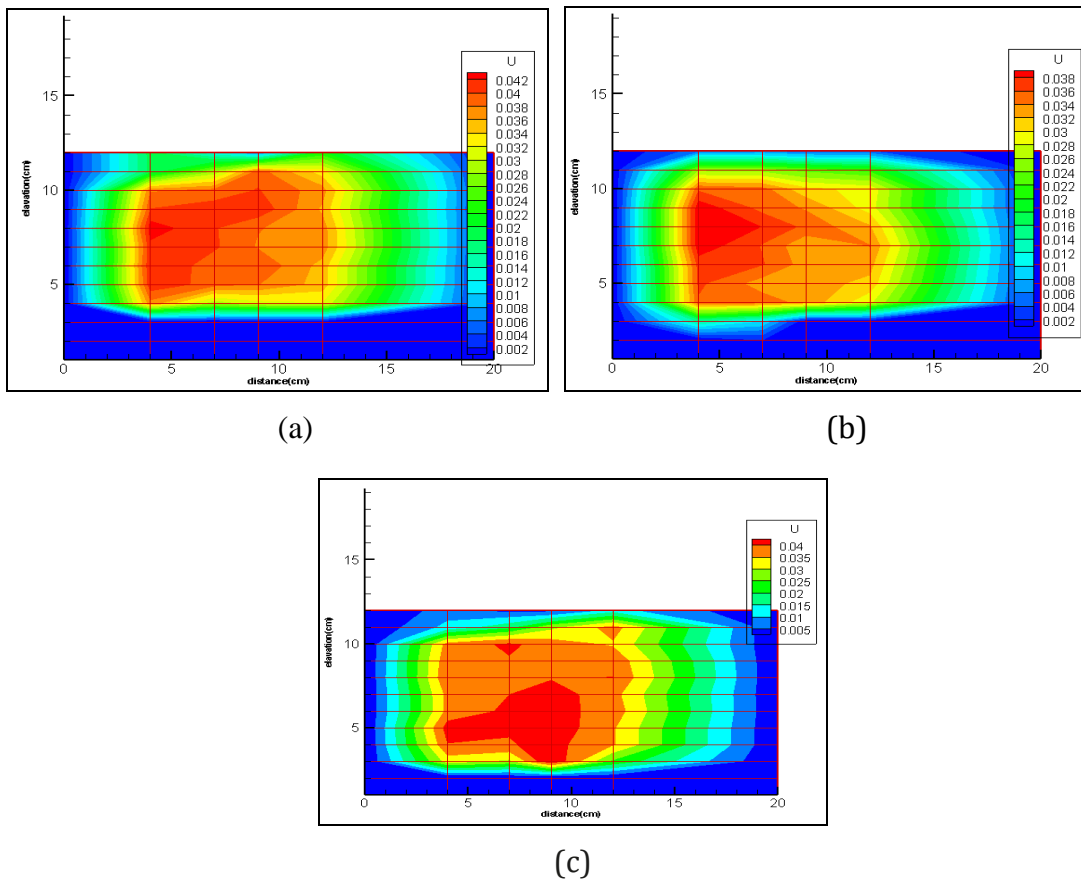


**Figure 16.** Velocity Cross Profile At: (a) The beginning (b) The middle and (c) The end, of the first bend with R/B=2

The secondary flow caused the maximum velocity approaching to the outer wall and the maximum velocity transmitted to the outer wall. This is seen in the transverse velocity profiles in the second and third bends. The shear stress variations were also based on the transverse velocity profile changes, in other words, to the middle of the bend, the greatest tension occurred in the inner wall, and then it was drawn to the outer wall (Figure 17). In each bend the location of the thickest deposit was always displaced laterally from the centerline toward the outer bank. According to the results, by increasing the flow strength, the form of the bed is formed, which also increases the roughness of the bed. In addition, the stress increased with the complete formation of the shape of bed form, and after that, gradually decreased the surface of the shape of bed form and reduced stress by washing the bed form.

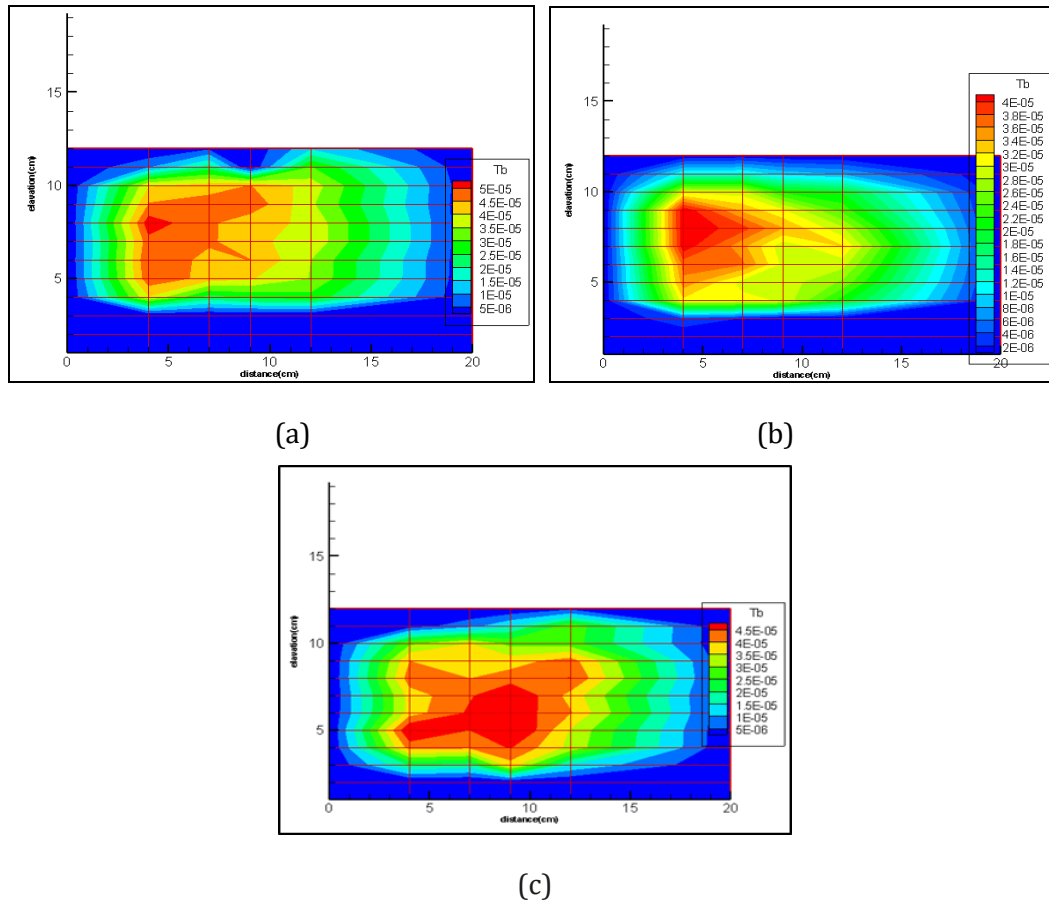


**Figure 17.** Shear Stress Profile At: (a) The beginning (b) The middle and (c) The end, of the first bend with  $R/B=2$

The position of the maximum velocity in the vertical direction of the velocity profile in a turbidity flow, depending on the Froude Number and the shear stress of the bed, can be observed near the bed instead of close to the top of the body of the turbidity flow. In the open channels, the velocity gradient increases rapidly from the bed to the surface of the water, and the maximum velocity occurs near the free surface of the water, while the flow velocity profile on the mobile bed occurs, upper than the bed (Figure 15). By increasing the radius of curvature, secondary flow can be poor and smaller. In other words maximum and minimum of secondary flow occur in bend with  $R/B=2$  and  $R/B=6$  respectively (Figure 18).

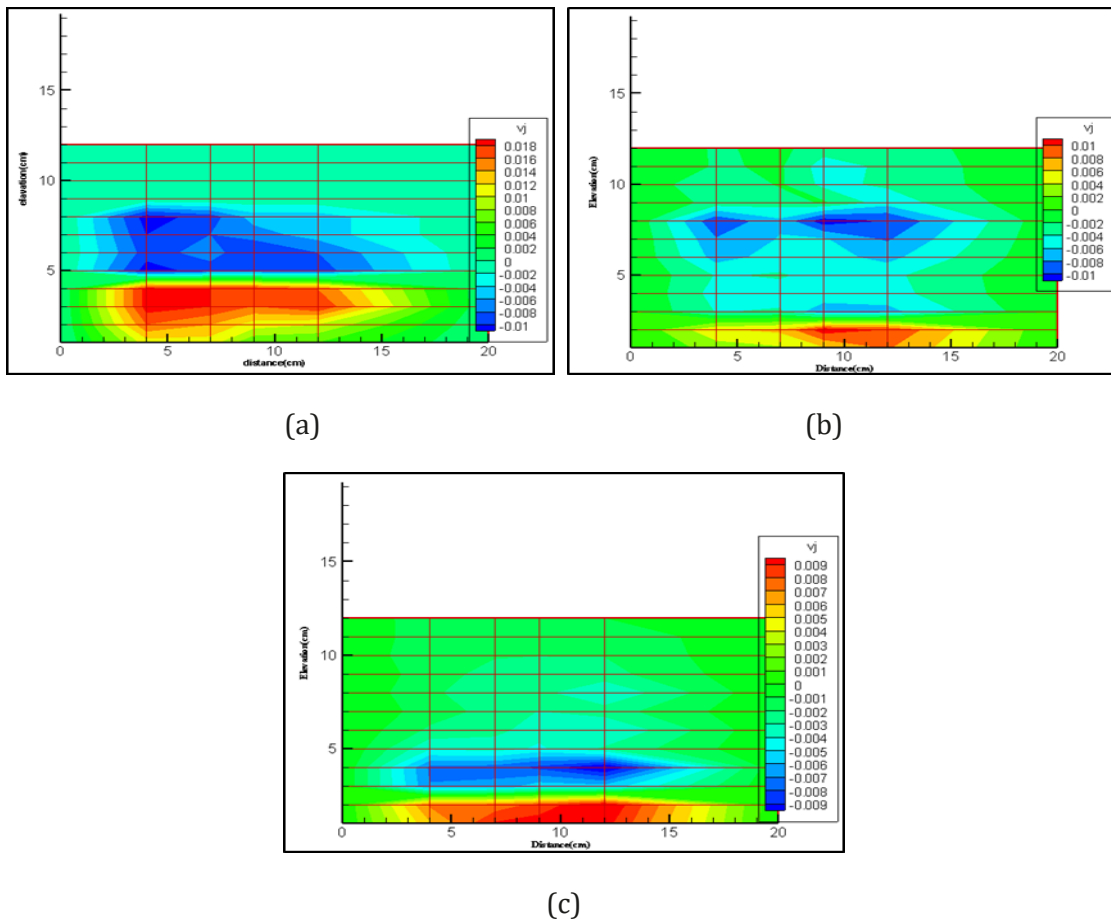


**Figure 18.** Secondary Flow Direction at The middle of: (a) the first bend (b)The second bend and (c) The third bend in run with  $Q=2.52l/s$ ,  $C=15gr/l$

The centrifugal force is inversely proportional to the curvature radius and as a result, with increasing radius of bend, the centrifugal force decreases. Reducing centrifugal force reduces the secondary flow. So the velocity of flow increase, and the depth of the flow is also reduced, due in the transverse sections of the third bend, the maximum longitudinal velocity and the lowest depth of the flow can be observed.

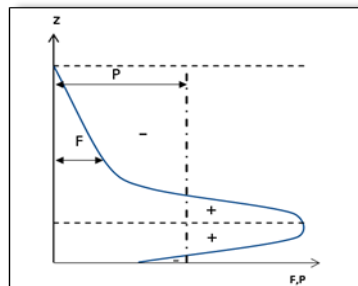


**Figure 19.** Diagram of Centrifugal Force and Pressure Force on unit volume of fluid in turbidity flow

According to (Figure 19), in a turbidity flow, we have two rotational cores in the bends: one is near the bed flume and the same as secondary flow in the open channel, and the other is

in the region above the maximum and reverse velocity. Unlike flow in open channels, the flow is drawn down to the outer bank; the direction of the secondary flow is inverted and from the inner bank to the outer bank.

## Conclusion

In turbidity current, the secondary flow results in the maximum velocity approaching to the outer wall and the maximum velocity is transferred to the outer wall. This is also observed in the transverse velocity profiles in the second and third bends. In general, on a mobile bed in a constant discharge, by increasing the concentration of inlet current, the flow velocity also increases. The important point in the flow rate profiles is that the rate of increase in velocity is for concentration increase, as it depends on changes in the bed form. As the concentration of turbidity flow increases, the shear stress of the bed is also increased. In mobile bed conditions, bed form particles are active and, with increasing speed and formation of bed forms, increase the roughness and resistance of the bed, so that the bed forms act as a force resistant to the flow of the inlet. According to the results, the flow rate will be reduced to about 19%. Accordingly, in the context of mobile bed conditions, it generally increased concentration due to increased flow velocity, and increased flow power and had the effect of changing the bed roughness and increasing the shear stress of the bed. In this sense, by washing the form of the bed form, the roughness and shear stress also begin to decrease. In all experiments, the forehead velocity increased in mobile bed conditions (by forming the bed form). Bed form particles are expected to be flammable agents. However, in these experiments, the introduction of foul deposition from the region of the cavity to the flow into the stream enhances the flow of the flow current and reduces the return flow to the flow resulting in an increase the forehead velocity about 14%. This illustrates the importance of forming a bed form for creating resistance to flow. Because of the fact that at the beginning of the current flow the bed form is not yet formed, and the agent of the resistivity and roughness of the bed is negligible, there is no resistance and decrease effect against the forehead velocity. According to the results of experiments on the mobile bed, increasing the concentration of the incoming flow, the flow velocity of the fluid is also increased. The important point in the flow rate profiles is that the rate of increase in velocity depends on changes in the form of the bed due to the increase in concentration. By increasing concentrations of turbidity flow, the shear stress of the bed is also increased. When the bed form was formed, as a result of it, the rate of velocity also increased at 25 g/l concentration and by increasing the shear stress, it decreased from 34% to 15%. Therefore, the rate of increase in velocity will occur by removing the bed forms and reducing the roughness and shear stress of the bed.

## Nomenclature

$\rho_s$  : density of the gravity flow [kg/m<sup>3</sup>]

$\rho_a$  : ambient fluid density [kg/m<sup>3</sup>]

$u_p$  : the peak velocity [m/s]

$h_p$ : the distance above the bed where this velocity is realized [m]

$u$ : averaged stream wise flow velocity [m/s]

$f_e$  :fractional excess density

$\Delta\rho$  : difference in density between the flow and the ambient water [ $\text{kg}/\text{m}^3$ ]

$u^*$  : bed shear velocity [ $\text{m}/\text{s}$ ]

$Fr_a$ :Densiometric Froude Number

$\tau$  = shear stress

$\rho$  = mass density of water [ $\text{kg}/\text{m}^3$ ]

$u'w'$  = covariance of velocity fluctuations in the stream-wise and vertical flow directions

$v'w'$  = covariance of velocity fluctuations in the transverse and vertical flow directions

$\phi_b$  = local angle of the scoured bed with the horizontal (equals 0 for plane bed)

$\tau_o$  = bed shear stress

$F_c$  = centrifugal force [ $\text{N}\cdot\text{m}/\text{s}^2$ ]

$m$  = mass of the moving object [N]

$v$  = moving velocity of the object [ $\text{m}/\text{s}$ ]

$r$  = value of the radius of curvature [m]

## References

Altinakar, MS, Graf, WH, Hopfinger, EJ. (1996). "Flow structure in turbidity currents." *J. Hydraul. Res.*, 34:713–718.

Buckee, C, Kneller, B, Peakall, J. (2001). "Turbulence structure in steady, solute-driven gravity currents." *Particulate gravity currents*, Special Publication of the International Association of Sediementologists 31, McCaffrey, WD, Kneller, BC, and Peakall, J. eds., Blackwell Science, Oxford, U.K., 31:173–187.

Chen, G, Shen, HS. (1984). River curvature-width ratio effect on shear stress. In: Elliott, C.M. (Ed.), *Proceedings Conference on Rivers*, New Orleans, LA., 687-699.

Dey, S, Barbhuiya, AK. (2005). Flow field at a vertical wall abutment. *Technical Notes, J. Hydraul. Eng.*, 131(12):1126-1135.

Duan, JG. (2009). Mean flow and turbulence around a laboratory spur dike. *J. Hydraul. Eng.*, 135(10):803-811.

Ellison, TH, Turner, JS. (1959). "Turbulent entrainment in stratified flows." *J. Fluid Mech.*, 6:423–448.

Richardson, E.V., Simons, D.B., Lagasse P.F. (2001). *River Engineering for Highway Encroachments*. Report No. FHWA NHI 01-004 HDS 6.

García, MH. (1993). "Hydraulic jumps in sediment-driven bottom currents." *J. Hydraul. Eng.*, 119:1094–1117.

- 
- García, MH. (1994). "Depositional Turbidity currents laden with poorly sorted sediment." *J. Hydraul. Eng.*, 12011:1240-1263.
- García, MH, Parker, G. (1993). "Experiments on the entrainment of sediment into suspension by a dense bottom current." *J. Geophys. Res., [Oceans]*, 98(C3):4793-4807.
- Huthnance, JM, Humphery, JD, Knight, PJ, Chatwin, G, Thomsen, L, White, M. (2002). Near-bed turbulence measurements, stress estimates and sediment mobility at the continental shelf edge. *Progres. Oceanog.*, 52:171-194.
- Ippen, AT, Drinker, PA, Jobin, WR, and Noutsopoulos, GK. (1962). "The Distribution of Boundary Shear Stresses in Curved Trapezoidal Channels." *J. Hydraulics Division*, 88(5):143-180.
- Keller, EA. (1971). Areal sorting of bed load material: the hypothesis of velocity reversal. *Bull. Geolog. Soc. Am.*, 82:753-756.
- Kneller, BC, Bennett, SJ, and McCaffrey, WD. (1999). "Velocity structure, turbulence and fluid stresses in experimental gravity currents." *J. Geophys. Res.*, 104(C3):5381-5391.
- Lofquist, K. (1960). "Flow and stress near an interface between stratified liquids." *Phys. Fluids*, 32, 158-175.
- Middleton, GV. (1966). "Experiments on density and turbidity currents, II. Uniform flow of density currents." *Can. J. Earth Sci.*, 3:627-637.
- Parker, G, Fukushima, Y, Pantin, HM. (1986). "Self-accelerating turbidity currents." *J. Fluid Mech.*, 171, 145-181.
- Parker, G, García, M, Fukushima, Y, Yu, W. (1987). "Experiments on turbidity currents over an erodible bed." *J. Hydraul. Res.*, 251:123-147.
- Sear, DA. (1996). Sediment transport in pool-riffle sequences. *Earth Surface Proces. Landform.*, 21:241-262.
- Sequeiros, OE, Naruse, H, Endo, N, García, MH, Parker, G. (2009). "Experimental study on self-accelerating turbidity currents." *J. Geophys. Res.*, 114:C05025. [doi.org/10.1029/2008JC005149](https://doi.org/10.1029/2008JC005149).
- Smith, R, Möller, N. (2003). Sedimentology and reservoir modelling of the Ormen Lange field, mid Norway. *Marine Petrol. Geology.*, 20:601-613.
- Tilston, M. (2005). Three-dimensional Flow Structure, Turbulence and Bank Erosion in a 1800 Meander Loop. Thesis, University of Montreal, Quebec, Canada.
- Xu, JP, Noble, MA, Rosenfeld, LK. (2004). "In-situ measurements of velocity structure within turbidity currents." *Geophys. Res. Lett.*, 31:L09311.
- Watson, CC, Biedenharn, DS, Thorne, C.R. (2005). Stream Rehabilitation. Version 1.0, 201 pp., Cottonwood Research, Fort Collins, Colorado.

---

Winn, RD, and Dott, RH, Jr. (1977). "Large-scale traction produced structures in deep-water fan channel conglomerates in southern Chile." *Geology*, 5:41-44.

**How to cite this article:** Marzieh Mohammadi, Mehdi Ghomeshi. Experimental Investigation of Turbidity Flow in 90 Degree Bend with Mobile Bed. *International Journal of Advanced Biological and Biomedical Research*, 2019, 7(4), 353-369. Link: <http://www.ijabbr.com/article 35665.html>